Seismoelectric reflection and transmission at a fluid/porous-medium interface

Menne Schakel[a] and David Smeulders
Department of Geotechnology, Delft University of Technology, 2600 GA Delft, The Netherlands

(Received 9 March 2009; revised 14 October 2009; accepted 14 October 2009)

The dispersion relation for seismoelectric wave propagation in poroelastic media is formulated in terms of effective densities comprising all viscous and electrokinetic coupling effects. Using Helmholtz decomposition, two seismoelectric conversion coefficients are derived, for an incident *P*-wave upon an interface between a compressible fluid and a poroelastic medium. These coefficients relate the incident *P*-wave to a reflected electromagnetic wave in the fluid, and a transmitted electromagnetic wave in the porous medium. The dependency on angle of incidence and frequency is computed. Using orthodox and interference fluxes, it is shown that energy conservation is satisfied. A sensitivity analysis indicates that electrolyte concentration, viscosity, and permeability highly influence seismoelectric conversion.
 [DOI: 10.1121/1.3263613]

PACS number(s): 43.20.El, 43.20.Gp, 43.40.Ph, 43.30.Ma [RR] Pages: 13–21

I. INTRODUCTION

When the grain surfaces of soils and rocks are in contact with a fluid electrolyte, they typically acquire a chemically bound surface charge that is balanced by mobile counterions in a thin fluid layer surrounding the grains. The bound charge is immobile, whereas the counterions can move. The distribution of mobile ions is determined by a balance between electrostatic forces and thermal diffusivity. At the interface between the immobile and counterions the so-called zeta-potential is defined. The potential varies exponentially when one moves away from the interface. The corresponding characteristic length scale is called the Debye length, which is on the order of some tens of nanometers for typical grain-electrolyte combinations (Pride, 1994). The ensemble of bound and mobile charge layers is referred to as the electrochemical double layer.

A compressional wave in fluid-saturated porous media will create pressure peaks and troughs on the scale of the wavelength. The resulting hydraulic flow will transport the counterions relative to the immobile, bound charge. In this way, counterions accumulate in pressure troughs and bound charge becomes exposed in pressure peaks, creating an electric coseismic field at the scale of the wavelength (Haines *et al.*, 2007). This electric field drives a conduction current that exactly balances the hydraulic current flow. Thus there is no net electric current for a propagating compressional wave within a homogeneous material. For interfaces, however, this is no longer the case. When a compressional or shear wave traverses an interface with a contrast in electrical or mechanical properties, an electric current imbalance is produced resulting in electromagnetic (EM)-waves that can propagate outside the support of the seismic waves (Haartsen and Pride, 1997). The generation of these waves at interfaces can thus be associated with new, electrokinetic, reflection, and transmission coefficients.

Several studies measured the conversion of seismic to electromagnetic energy in the field (Thompson and Gist, 1993; Butler *et al.*, 1996; Mikhailov *et al.*, 1997; Garambois and Dietrich, 2001; Haines *et al.*, 2007). The inverse electroseismic conversion was also measured (Thompson *et al.*, 2007; Zhu *et al.*, 2008). So-called electroseismograms in layered media were presented by several authors (e.g., Haartsen and Pride, 1997; Han and Wang, 2001; White and Zhou, 2006; Haines and Pride, 2006). In order to obtain the electrokinetic reflection and transmission coefficients at a fluid/porous-medium interface Block and Harris (2006) approximated Pride's (1994) electrokinetic theory by solving the Biot reflection problem only, from which the relative pore fluid flow is obtained. This flow subsequently acts as a source term in the EM boundary conditions of Pride's (1994) theory. In this paper, we solve the complete boundary value problem in a procedure similar to Denneman *et al.* (2002), where an acoustic wave from a compressible fluid impinges on a poroelastic medium. Two new parameters are defined, describing the conversion from seismic to EM-waves. The incident fluid wave is transmitted into fast and slow compressional waves, a shear wave, and into an EM-wave. Part of the incident wave is reflected as a fluid wave and a fluid EM-wave. In Sec. II we introduce the governing equations and we present the electrokinetic dispersion relations. The dependency of the seismoelectric reflection and transmission coefficients on angle of incidence and frequency is derived in Sec. III. In Sec. IV we recast the reflection and transmission coefficients in vertical energy flux coefficients and perform a sensitivity analysis.

II. GOVERNING EQUATIONS

We consider a poroelastic matrix saturated by an electrolyte and adopt an $\exp[i\omega t]$ convention for time varying

[a]Author to whom correspondence should be addressed. Electronic mail: m.d.schakel@tudelft.nl

fields. The governing linearized equations in an isotropic, homogeneous poroelastic medium were given by Pride and Haartsen (1996). We rewrite the equations here in a somewhat different form because we aim to derive the dispersion relations in terms of effective densities. We will confirm full consistency with the original Pride equations in the forthcoming. The governing equations read as

$$-\nabla\cdot\hat{\underline{\underline{\boldsymbol{\sigma}}}}-(1-\phi)\nabla\hat{p}=-\omega^2[\rho_{11}(\omega)\hat{\mathbf{u}}+\rho_{12}(\omega)\hat{\mathbf{U}}]+\frac{\eta\phi L(\omega)}{k(\omega)}\hat{\mathbf{E}}, \tag{1}$$

$$-\phi\nabla\hat{p}=-\omega^2[\rho_{12}(\omega)\hat{\mathbf{u}}+\rho_{22}(\omega)\hat{\mathbf{U}}]-\frac{\eta\phi L(\omega)}{k(\omega)}\hat{\mathbf{E}}, \tag{2}$$

$$\hat{\underline{\underline{\boldsymbol{\sigma}}}}=-G[\nabla\hat{\mathbf{u}}+(\nabla\hat{\mathbf{u}})^T]-\left[\left(A-Q\frac{1-\phi}{\phi}\right)\nabla\cdot\hat{\mathbf{u}}+\left(Q-R\frac{1-\phi}{\phi}\right)\nabla\cdot\hat{\mathbf{U}}\right]\underline{\underline{\mathbf{I}}}, \tag{3}$$

$$\hat{p}=-\frac{1}{\phi}(Q\nabla\cdot\hat{\mathbf{u}}+R\nabla\cdot\hat{\mathbf{U}}), \tag{4}$$

$$\hat{\mathbf{J}}=\sigma(\omega)\hat{\mathbf{E}}+L(\omega)(-\nabla\hat{p}+\omega^2\rho_f\hat{\mathbf{u}}), \tag{5}$$

$$\nabla\times\hat{\mathbf{H}}=i\omega\varepsilon\hat{\mathbf{E}}+\hat{\mathbf{J}}, \tag{6}$$

$$\nabla\times\hat{\mathbf{E}}=-i\omega\mu\hat{\mathbf{H}}. \tag{7}$$

Hats over field variables indicate small frequency-domain quantities, ω is the angular frequency, η is the pore fluid viscosity, ϕ is the porosity, ρ_f is the pore fluid density, μ is the magnetic permeability, ε is the bulk electrical permittivity given by $\varepsilon=\varepsilon_0[\phi(\epsilon_f-\epsilon_s)/\alpha_\infty+\epsilon_s]$, with solid and pore fluid relative permittivities ϵ_s and ϵ_f, and vacuum permittivity ε_0. $\underline{\underline{\mathbf{I}}}$ denotes the identity matrix. The field variables are solid and (pore) fluid displacements $\mathbf{u}$ and $\mathbf{U}$, intergranular stress $\underline{\underline{\boldsymbol{\sigma}}}$, pore pressure p, electric current density $\mathbf{J}$, and the electric and magnetic fields $\mathbf{E}$ and $\mathbf{H}$. A, Q, and R are the generalized elastic coefficients that are related to the bulk modulus of the skeleton grains K_s, the shear modulus G, the bulk modulus of the pore fluid K_f, and the bulk modulus of the framework of grains K_b as follows (Biot and Willis, 1957):

$$A=\frac{(1-\phi)^2K_sK_f-(1-\phi)K_bK_f+\phi K_sK_b}{K_f\left(1-\phi-\frac{K_b}{K_s}\right)+\phi K_s}-\frac{2}{3}G, \tag{8}$$

$$Q=\frac{\phi[K_s(1-\phi)-K_b]K_f}{K_f\left(1-\phi-\frac{K_b}{K_s}\right)+\phi K_s}, \tag{9}$$

$$R=\frac{\phi^2K_sK_f}{K_f\left(1-\phi-\frac{K_b}{K_s}\right)+\phi K_s}. \tag{10}$$

The dynamic permeability $k(\omega)$ describes the transition from viscosity toward inertia-dominated flow. The electrokinetic coupling coefficient $L(\omega)$ couples mechanical and EM-wave behavior. Note that for $L(\omega)=0$, mechanical and EM-fields are decoupled in Eqs. (1)–(7). Equations (1)–(4) then transform into the original Biot equations (Biot, 1956a, 1956b) and Eqs. (5)–(7) into Ohm's law and Maxwell's equations. The conductivity of the pore fluid is denoted as $\sigma(\omega)$. Expressions for $k(\omega)$, $L(\omega)$, and $\sigma(\omega)$ are given in Appendix A. As the dynamic permeability and the fluid and solid density terms always appear together, it is convenient to define effective densities $\rho_{11}(\omega)$, $\rho_{12}(\omega)$, and $\rho_{22}(\omega)$ as follows:

$$\rho_{11}(\omega)=(1-\phi)\rho_s-\rho_{12}(\omega), \tag{11}$$

$$\rho_{12}(\omega)=\phi\rho_f\left[1+i\frac{\phi\eta}{\omega\rho_fk(\omega)}\right], \tag{12}$$

$$\rho_{22}(\omega)=\phi\rho_f-\rho_{12}(\omega), \tag{13}$$

where ρ_s is the solid density. Adding Eqs. (1) and (2), we obtain the original dynamic equation (3) by Pride and Haartsen (1996) (no source term). With the definitions for $\rho_{12}(\omega)$ and $\rho_{22}(\omega)$, Eq. (2) is written as

$$i\omega\phi(\hat{\mathbf{U}}-\hat{\mathbf{u}})=L(\omega)\hat{\mathbf{E}}+\frac{k(\omega)}{\eta}(-\nabla\hat{p}+\omega^2\rho_f\hat{\mathbf{u}}), \tag{14}$$

which is Eq. (5) from Pride and Haartsen (1996) (no source term). By adding Eqs. (3) and (4), we obtain an expression for total stress $\underline{\underline{\boldsymbol{\tau}}}=-\underline{\underline{\boldsymbol{\sigma}}}-p\underline{\underline{\mathbf{I}}}$, which corresponds to Eq. (6) by Pride and Haartsen (1996). Full consistency with the original Pride equations is thus confirmed.

Substituting Eqs. (3) and (4) into Eqs. (1) and (2) yields

$$G\nabla^2\hat{\mathbf{u}}+(A+G)\nabla\nabla\cdot\hat{\mathbf{u}}+Q\nabla\nabla\cdot\hat{\mathbf{U}}=-\omega^2[\rho_{11}(\omega)\hat{\mathbf{u}}+\rho_{12}(\omega)\hat{\mathbf{U}}]+\frac{\eta\phi L(\omega)}{k(\omega)}\hat{\mathbf{E}}, \tag{15}$$

$$Q\nabla\nabla\cdot\hat{\mathbf{u}}+R\nabla\nabla\cdot\hat{\mathbf{U}}=-\omega^2[\rho_{12}(\omega)\hat{\mathbf{u}}+\rho_{22}(\omega)\hat{\mathbf{U}}]-\frac{\eta\phi L(\omega)}{k(\omega)}\hat{\mathbf{E}}. \tag{16}$$

Eliminating $(-\nabla\hat{p}+\omega^2\rho_f\hat{\mathbf{u}})$ from Eqs. (5) and (14) we obtain

$$i\omega\phi(\hat{\mathbf{U}}-\hat{\mathbf{u}})=L(\omega)\hat{\mathbf{E}}+\frac{k(\omega)}{\eta}\left(\frac{\hat{\mathbf{J}}-\sigma(\omega)\hat{\mathbf{E}}}{L(\omega)}\right). \tag{17}$$

Substituting Eq. (6) into Eq. (17) we obtain

$$i\omega\phi(\hat{\mathbf{U}}-\hat{\mathbf{u}})=L(\omega)\hat{\mathbf{E}}+\frac{k(\omega)}{\eta L(\omega)}\left(\nabla\times\hat{\mathbf{H}}-[i\omega\varepsilon+\sigma(\omega)]\hat{\mathbf{E}}\right). \tag{18}$$

Finally, substituting Eq. (7) into Eq. (18) we obtain

TABLE I. Parameters of the poroelastic medium and fluid. Parameters of poroelastic medium from Denneman *et al.* (2002).

Parameters poroelastic medium	
Bulk modulus framework of grains, K_b	5.8×10^9 Pa
Shear modulus framework of grains, G	3.4×10^9 Pa
Bulk modulus skeleton grains, K_s	40×10^9 Pa
Bulk modulus pore fluid, K_f	2.22×10^9 Pa
Pore fluid viscosity, η	0.001 Pa s
Pore fluid density, ρ_f	1000 kg/m^3
Solid density, ρ_s	2760 kg/m^3
Tortuosity of the porous medium, α_∞	2.3
Porosity of the porous medium, ϕ	0.24
Permeability, k_0	0.390×10^{-12} m^2
Temperature, T	295 K
Hydrogen exponent, pH	7
Relative permittivity of the pore fluid, ϵ_f	80
Relative permittivity of the solid, ϵ_s	4
Magnetic permeability ($=\mu_0$), μ	$4\pi\times10^{-7}$ H/m
Valence of species-1 ion, z_1	1
Valence of species-2 ion, z_2	–1
Mobility of species-1 ion, b_1 [a]	3.246×10^{11} m/(N s)
Mobility of species-2 ion, b_2 [a]	4.931×10^{11} m/(N s)
Zeta-potential, ζ [b]	–0.065 V
Similarity parameter, M	1
Concentration of the electrolyte, C	0.001 mol/l
Parameters fluid	
Bulk modulus fluid, K_{fl}	2.22×10^9 Pa
Fluid density, ρ_{fl}	1000 kg/m^3
Fluid relative permittivity, ϵ_{fl}	80
Fluid magnetic permeability ($=\mu_0$), μ_{fl}	$4\pi\times10^{-7}$ H/m
Fluid conductivity, σ_{fl}	5.0×10^{-3} S/m

[a]Nabighian and Corbett, 1988.
[b]From Eq. (A5).

$$\omega^2\mu\bar{\varepsilon}(\omega)\hat{\mathbf{E}}+\omega^2\mu\frac{\eta\phi L(\omega)}{k(\omega)}(\hat{\mathbf{U}}-\hat{\mathbf{u}})=\nabla\nabla\cdot\hat{\mathbf{E}}-\nabla^2\hat{\mathbf{E}}, \quad (19)$$

where $\bar{\varepsilon}(\omega)$ is the newly defined effective electrical permittivity

$$\bar{\varepsilon}(\omega)=\varepsilon-i\frac{\sigma(\omega)}{\omega}+i\frac{\eta L^2(\omega)}{\omega k(\omega)}. \quad (20)$$

Equations (15), (16), and (19) form a closed set of equations for the fields **u**, **U**, and **E**. A summary of electrokinetic symbols is given in Table I.

A. Electrokinetic wave velocities

Electrokinetic theory in isotropic, homogeneous media predicts the existence of uncoupled longitudinal and transversal modes. There are two longitudinal waves, the fast *P*-wave and the slow *P*-wave, and two transversal waves: an electromagnetic wave and a seismic shear wave (Pride and Haartsen, 1996). We derive complex electrokinetic wave velocities in a procedure similar to that of Allard (1993). First, we define the following Helmholtz decompositions:

$$\hat{\mathbf{u}}=\nabla\hat{\varphi}_s+\nabla\times\hat{\boldsymbol{\Psi}}_s, \quad (21)$$

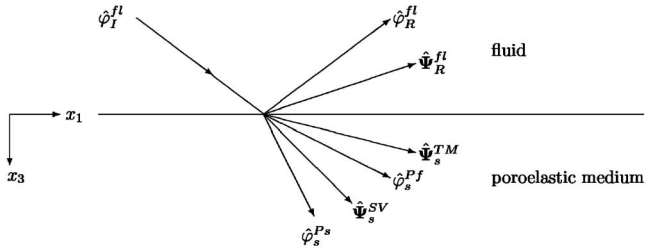

FIG. 1. Seismoelectric reflection and transmission potentials due to an incident fluid wave.

$$\hat{\mathbf{U}}=\nabla\hat{\varphi}_f+\nabla\times\hat{\boldsymbol{\Psi}}_f, \quad (22)$$

$$\hat{\mathbf{E}}=\nabla\hat{\varphi}_E+\nabla\times\hat{\boldsymbol{\Psi}}_E. \quad (23)$$

These are substituted in Eqs. (15), (16), and (19). This yields two separate sets: one for the longitudinal waves and one for the transversal waves. Subsequently, plane wave propagation is introduced in the $(x_1,0,x_3)$ plane (see Fig. 1), e.g., $\hat{\varphi}_s=\tilde{\varphi}_s\exp[-i\mathbf{k}\cdot\mathbf{x}]$ and $\hat{\boldsymbol{\Psi}}_s=(0,\tilde{\psi}_s\exp[-i\mathbf{k}\cdot\mathbf{x}],0)^T$, where **k** is the wavenumber vector and **x** is the position vector in that plane. Through elimination of $\tilde{\varphi}_E$ in the longitudinal wave equations a system of equations for $\tilde{\varphi}_s$ and $\tilde{\varphi}_f$ is obtained. The nontrivial solution yields the squared complex slowness (i.e., inverse complex-valued wave velocities) of the longitudinal waves $s_l^2(\omega)$

$$s_l^2(\omega)=\frac{-d_1(\omega)}{2d_2}\mp\frac{1}{2}\sqrt{\left[\frac{d_1(\omega)}{d_2}\right]^2-4\frac{d_0(\omega)}{d_2}}, \quad (24)$$

where $l=Pf, Ps$ refers to the fast and slow longitudinal waves, respectively, and

$$d_0(\omega)=\bar{\rho}_{11}(\omega)\bar{\rho}_{22}(\omega)-[\bar{\rho}_{12}(\omega)]^2,$$

$$d_1(\omega)=-[P\bar{\rho}_{22}(\omega)+R\bar{\rho}_{11}(\omega)-2Q\bar{\rho}_{12}(\omega)],$$

$$d_2=PR-Q^2, \quad (25)$$

where $P=A+2G$. As the effective densities and the electrokinetic coupling factor always appear together, it is convenient to define new effective densities $\bar{\rho}_{11}(\omega)$, $\bar{\rho}_{12}(\omega)$, and $\bar{\rho}_{22}(\omega)$ as follows:

$$\bar{\rho}_{11}(\omega)=\rho_{11}(\omega)-E_K(\omega), \quad (26)$$

$$\bar{\rho}_{12}(\omega)=\rho_{12}(\omega)+E_K(\omega), \quad (27)$$

$$\bar{\rho}_{22}(\omega)=\rho_{22}(\omega)-E_K(\omega), \quad (28)$$

$$E_K(\omega)=\frac{\eta^2\phi^2L^2(\omega)}{k^2(\omega)\bar{\varepsilon}(\omega)\omega^2}. \quad (29)$$

We note that both viscous and electrokinetic coupling effects are now elegantly comprised in effective frequency-dependent densities.

A similar approach is used for the transversal waves. Through elimination of $\tilde{\boldsymbol{\Psi}}_E$ in the transversal wave equations, a system of equations for $\tilde{\boldsymbol{\Psi}}_s$ and $\tilde{\boldsymbol{\Psi}}_f$ is obtained. The nontrivial solution yields the squared complex slowness of

the transversal waves $s_l^2(\omega)$ according to Eq. (24), where now $l=EM, S$ refers to the EM and seismic shear waves, respectively, and

$$d_0(\omega) = \mu\bar{\varepsilon}(\omega)\frac{\bar{\rho}_{11}(\omega)\bar{\rho}_{22}(\omega) - [\bar{\rho}_{12}(\omega)]^2}{G},$$

$$d_1(\omega) = -\mu\bar{\varepsilon}(\omega)\bar{\rho}_{22}(\omega) - \frac{\rho_{11}(\omega)\rho_{22}(\omega) - [\rho_{12}(\omega)]^2}{G},$$

$$d_2(\omega) = \rho_{22}(\omega). \tag{30}$$

From the complex-valued slowness, phase velocities and attenuation coefficients are readily obtained.

III. REFLECTION AND TRANSMISSION AT A PLANE FLUID/POROUS-MEDIUM INTERFACE

A compressible fluid overlays an isotropic, homogeneous porous medium. The horizontal interface is at $x_3=0$ (see Fig. 1). We adopt a right-hand (x_1,x_2,x_3) coordinate system with the x_3-axis pointing downward. A plane fluid wave (scalar potential $\hat{\varphi}_I^{fl}$) impinges on the interface where it reflects as a P-wave (scalar potential $\hat{\varphi}_R^{fl}$) and a transverse magnetic (*TM*) EM-wave (vector potential $\hat{\mathbf{\Psi}}_R^{fl}$). It transmits as a *TM*-wave (vector potential $\hat{\mathbf{\Psi}}_s^{TM}$), a fast longitudinal wave (scalar potential $\hat{\varphi}_s^{Pf}$), a slow longitudinal wave (scalar potential $\hat{\varphi}_s^{Ps}$), and a vertical shear (*SV*)-wave (vector potential $\hat{\mathbf{\Psi}}_s^{SV}$). The reflection and transmission coefficients are obtained from the (open-pore) boundary conditions, which are continuity of fluid volume displacement, fluid pressure, the horizontal magnetic and electric fields, and vanishing vertical and horizontal intergranular stresses (Deresiewicz and Skalak, 1963; Pride and Haartsen, 1996)

$$(1-\phi)\hat{u}_3 + \phi\hat{U}_3 = \hat{U}_3^{fl}, \tag{31}$$

$$\hat{p} = \hat{p}^{fl}, \tag{32}$$

$$\hat{\sigma}_{13} = \hat{\sigma}_{33} = 0, \tag{33}$$

$$\hat{H}_2 = \hat{H}_2^{fl}, \tag{34}$$

$$\hat{E}_1 = \hat{E}_1^{fl}. \tag{35}$$

The pressure in the upper fluid layer is denoted by p^{fl}. Magnetic and electric fields in the upper fluid layer are indicated by $\mathbf{H}^{fl}$ and $\mathbf{E}^{fl}$, respectively. We relate p^{fl} to upper fluid layer displacement $\mathbf{U}^{fl}$ by $p^{fl}=-K_{fl}\nabla\cdot\mathbf{U}^{fl}$, where K_{fl} is the bulk modulus of the upper fluid layer. The upper fluid layer wave speed c is related to the upper layer fluid density ρ_{fl} by $c=\sqrt{K_{fl}/\rho_{fl}}$. Viscosity does not play a role in the overlying fluid because the ratio of viscous and inertia terms is $\eta\omega/c^2\rho_{fl}$, which is on the order $10^{-11}-10^{-6}$ for the frequencies considered in this paper.

Scalar potentials $\hat{\varphi}_s$, $\hat{\varphi}_f$, and $\hat{\varphi}_E$, see Eqs. (21)–(23), are composed of contributions of the longitudinal waves, e.g., $\hat{\varphi}_s=\hat{\varphi}_s^{Pf}+\hat{\varphi}_s^{Ps}$, and, similarly, vector potentials $\hat{\mathbf{\Psi}}_s$, $\hat{\mathbf{\Psi}}_f$, and $\hat{\mathbf{\Psi}}_E$ are composed of contributions of the transversal waves, e.g., $\hat{\mathbf{\Psi}}_s=\hat{\mathbf{\Psi}}_s^{TM}+\hat{\mathbf{\Psi}}_s^{SV}=(0,\hat{\psi}_s^{TM},0)^T+(0,\hat{\psi}_s^{SV},0)^T$. The dispersion relations given in Eq. (24) not only predict the phase velocities and attenuation coefficients, but also the fluid-solid amplitude ratios β^m and β^n and the amplitude ratios α^m and α^n $(\mathrm{V/m^2})$ that describe the strength of the electric field with respect to the solid displacement amplitude, for each wave

$$\beta^m(\omega) = \frac{\hat{\varphi}_f^m}{\hat{\varphi}_s^m} = \frac{\bar{\rho}_{11}(\omega) - Ps_m^2(\omega)}{Qs_m^2(\omega) - \bar{\rho}_{12}(\omega)}, \tag{36}$$

$$\beta^n(\omega) = \frac{\hat{\psi}_f^n}{\hat{\psi}_s^n} = \frac{Gs_n^2(\omega) - (1-\phi)\rho_s}{\phi\rho_f}, \tag{37}$$

$$\alpha^m(\omega) = \frac{\hat{\varphi}_E^m}{\hat{\varphi}_s^m} = \frac{\eta\phi L(\omega)}{k(\omega)\bar{\varepsilon}(\omega)}[1-\beta^m(\omega)], \tag{38}$$

$$\alpha^n(\omega) = \frac{\hat{\psi}_E^n}{\hat{\psi}_s^n} = \frac{\mu\eta\phi L(\omega)}{k(\omega)[\mu\bar{\varepsilon}(\omega) - s_n^2(\omega)]}[1-\beta^n(\omega)], \tag{39}$$

for $m=Pf$ or Ps, and $n=TM$ or SV. We now specify the following plane wave propagation expressions:

$$\hat{\varphi}_I^{fl} = \tilde{\varphi}_I^{fl}\exp[-i(k_1x_1 + k_3^{fl}x_3)], \tag{40}$$

$$\hat{\varphi}_R^{fl} = \tilde{\varphi}_R^{fl}\exp[-i(k_1x_1 - k_3^{fl}x_3)], \tag{41}$$

$$\hat{\mathbf{\Psi}}_R^{fl} = (0,\tilde{\psi}_R^{fl}\exp[-i(k_1x_1 - k_3^{E}x_3)],0)^T, \tag{42}$$

$$\hat{\varphi}_s^m = \tilde{\varphi}_s^m\exp[-i(k_1x_1 + k_3^{m}x_3)], \tag{43}$$

$$\hat{\mathbf{\Psi}}_s^n = (0,\tilde{\psi}_s^n\exp[-i(k_1x_1 + k_3^{n}x_3)],0)^T, \tag{44}$$

where k_3^{fl} and k_3^E are the vertical wavenumbers of the incident fluid wave and reflected EM-wave, respectively. The reflection and transmission coefficients are

$$R^E = \frac{\tilde{\psi}_R^{fl}}{\tilde{\varphi}_I^{fl}}, \quad R^M = \frac{\tilde{\varphi}_R^{fl}}{\tilde{\varphi}_I^{fl}}, \quad T^{Pf} = \frac{\tilde{\varphi}_s^{Pf}}{\tilde{\varphi}_I^{fl}},$$

$$T^{Ps} = \frac{\tilde{\varphi}_s^{Ps}}{\tilde{\varphi}_I^{fl}}, \quad T^{TM} = \frac{\tilde{\psi}_s^{TM}}{\tilde{\varphi}_I^{fl}}, \quad T^{SV} = \frac{\tilde{\psi}_s^{SV}}{\tilde{\varphi}_I^{fl}}, \tag{45}$$

where R^M indicates the mechanical reflection coefficient and R^E indicates the seismoelectric reflection coefficient. Applying boundary conditions (31)–(35) yields a linear system of six equations and six unknowns

$$\underline{\underline{\mathbf{A}}}\cdot(R^E,R^M,T^{Pf},T^{Ps},T^{TM},T^{SV})^T = (k_3^{fl},\phi\rho_{fl},0,0,0,0)^T, \tag{46}$$

where elements of matrix $\underline{\underline{\mathbf{A}}}$ are given in Appendix B. We solve Eq. (46) by Cramer's rule and show the results for R^E and T^{TM} as a function of incidence angle θ at a fixed frequency of 10 Hz in Fig. 2. The parameter values, representative for a water/shallow-sandstone interface, are given in Table I. We use these values in all computations of the reflection and transmission coefficients. For sin θ between $\sim$0 and $\sim$0.6, $|R^E|$ is approximately constant. Note that for

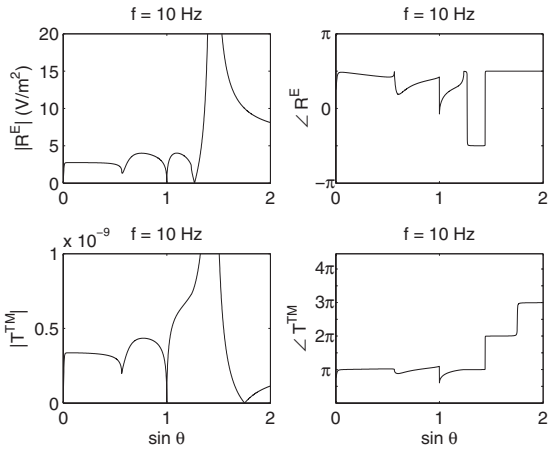

FIG. 2. Amplitudes (left) and phase values (right) of seismoelectric reflection (R^E) and transmission (T^{TM}) coefficients at a fluid/porous-medium boundary.

sin θ=0, no reflected EM-wave is generated due to the prescribed boundary conditions. For the parameters of Table I, $|R^E|$ is approximately 3 V/m^2, which is equivalent to $\sim 8 \times 10^{-7}$ V/Pa at 10 Hz. At sin $\theta \approx 0.57$, $|R^E|$ has a local minimum associated with critical reflection of the fast *P*-wave. Obviously, sin θ=1 corresponds to grazing angle of incidence and there is no seismoelectric conversion ($|R^E|$=0). We associate sin $\theta \approx 1.24$ with critical reflection of the SV-wave and we associate the peak at sin $\theta \approx 1.44$ with the Stoneley wave. The above mentioned behavior is also visible in the phase behavior of R^E, and the behavior of T^{TM}. At sin θ=0 and sin θ=1, R^E and T^{TM} are identically zero. We note that generally $|T^{TM}|$ is on the order 10^{-10}.

Next we show in Fig. 3 the frequency-dependence of $|R^E|$ and $|T^{TM}|$ for 45° angle of incidence. Both seismoelectric coefficients increase strongly with frequency, which corresponds to increasing EM-wave velocities in the diffusive regime for both the fluid and poroelastic medium. We note that the increase in $|T^{TM}|$ sharply diminishes at $\omega=\omega_t$, i.e., for the frequency that separates viscosity-dominated flow from inertia-dominated flow.

IV. SENSITIVITY ANALYSIS

A natural way to perform a sensitivity analysis is to analyze the ratio of reflected/transmitted wave energy fluxes to the incident flux; see, e.g., Dutta and Odé (1983) and Santos *et al.* (1992).

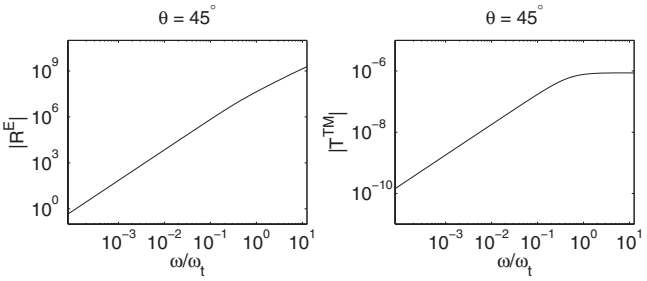

FIG. 3. Magnitude of seismoelectric coefficients R^E and T^{TM} as a function of normalized frequency at θ=45° angle of incidence.

A. Vertical electrokinetic energy fluxes

The electrokinetic vertical energy flux $Y_3(\mathbf{x},t)$ of the porous medium, defined by the dot product of the Poynting vector $\mathbf{Y}$ and the unit normal to the interface $\mathbf{n}=(0,0,1)^T$, is given by (Haartsen, 1995)

$$\begin{aligned} Y_3(\mathbf{x},t) &= [\mathbf{E}(\mathbf{x},t) \times \mathbf{H}(\mathbf{x},t) + \underline{\boldsymbol{\tau}}(\mathbf{x},t) \cdot \dot{\mathbf{u}}(\mathbf{x},t) \\ &\quad - \phi p(\mathbf{x},t)\big(\dot{\mathbf{U}}(\mathbf{x},t) - \dot{\mathbf{u}}(\mathbf{x},t)\big)] \cdot \mathbf{n} \\ &= E_1(\mathbf{x},t)H_2(\mathbf{x},t) + \tau_{31}(\mathbf{x},t)\dot{u}_1(\mathbf{x},t) \\ &\quad + \tau_{33}(\mathbf{x},t)\dot{u}_3(\mathbf{x},t) - \phi p(\mathbf{x},t) \\ &\quad \times \big(\dot{U}_3(\mathbf{x},t) - \dot{u}_3(\mathbf{x},t)\big). \end{aligned} \tag{47}$$

Similar expressions to Eq. (47) were provided by Pride and Haartsen (1996), Dutta and Odé (1983), and Santos *et al.*, (1992). We note that in our geometry (see Fig. 1) $H_1(\mathbf{x},t) = E_2(\mathbf{x},t) = \tau_{32}(\mathbf{x},t) = u_2(\mathbf{x},t) = 0$. We now write real parts of all frequency-domain variables and calculate a time-average over 1 cycle in time so that $\langle Y_3(\mathbf{x},t)\rangle$ becomes

$$\begin{aligned} \langle Y_3(\mathbf{x},t)\rangle &= \frac{1}{2\pi}\int_0^{2\pi} \Big(\mathrm{Re}\big[\hat{E}_1 \exp[i\omega t]\big]\mathrm{Re}\big[\hat{H}_2 \exp[i\omega t]\big] \\ &\quad + \mathrm{Re}\big[\hat{\tau}_{31} \exp[i\omega t]\big]\mathrm{Re}\big[i\omega\hat{u}_1 \exp[i\omega t]\big] \\ &\quad + \mathrm{Re}\big[\hat{\tau}_{33} \exp[i\omega t]\big]\mathrm{Re}\big[i\omega\hat{u}_3 \exp[i\omega t]\big] \\ &\quad - \mathrm{Re}\big[\hat{p} \exp[i\omega t]\big]\mathrm{Re}\big[i\omega\phi(\hat{U}_3 - \hat{u}_3) \\ &\quad \times \exp[i\omega t]\big]\Big) d(\omega t) \\ &= \frac{1}{2}[\hat{E}_1'\hat{H}_2' + \hat{E}_1''\hat{H}_2''] + \frac{\omega}{2}[\hat{\tau}_{31}''\hat{u}_1' - \hat{\tau}_{31}'\hat{u}_1''] \\ &\quad + \frac{\omega}{2}[\hat{\tau}_{33}''\hat{u}_3' - \hat{\tau}_{33}'\hat{u}_3''] - \frac{\omega}{2}[\phi\hat{p}''(\hat{U}_3' - \hat{u}_3') \\ &\quad - \phi\hat{p}'(\hat{U}_3'' - \hat{u}_3'')], \end{aligned} \tag{48}$$

where single and double primes denote real and imaginary parts of complex quantities, respectively. Denoting complex conjugation by an asterisk, we find that

$$\begin{aligned} \langle Y_3(\mathbf{x},t)\rangle &= \tfrac{1}{4}\Big\{(\hat{E}_1\hat{H}_2^\star + \hat{E}_1^\star\hat{H}_2) - i\omega\Big[(\hat{\tau}_{31}\hat{u}_1^\star - \hat{\tau}_{31}^\star\hat{u}_1) \\ &\quad + (\hat{\tau}_{33}\hat{u}_3^\star - \hat{\tau}_{33}^\star\hat{u}_3) - \big(\phi\hat{p}(\hat{U}_3^\star - \hat{u}_3^\star) \\ &\quad - \phi\hat{p}^\star(\hat{U}_3 - \hat{u}_3)\big)\Big]\Big\}. \end{aligned} \tag{49}$$

Each of the components in Eq. (49) is composed of contributions from the four electrokinetic waves, e.g., $\hat{E}_1 = \hat{E}_1^{Pf} + \hat{E}_1^{Ps} + \hat{E}_1^{TM} + \hat{E}_1^{SV}$. Writing all terms in Eq. (49) in separate contributions from each of the waves, we will have four orthodox fluxes, resulting from wave amplitudes multiplied by themselves, and six interference fluxes, resulting from cross-terms (Dutta and Odé, 1983; Santos *et al.*, 1992). In the non-dissipative fluid layer there is only an orthodox reflected EM-flux $\langle Y_3^{fl}(\mathbf{x},t)\rangle^{E,E}$, and incident and reflected orthodox acoustic fluxes $\langle Y_3^{fl}(\mathbf{x},t)\rangle^{Pin,Pin}$ and $\langle Y_3^{fl}(\mathbf{x},t)\rangle^{Pr,Pr}$. Vertical energy flux conservation requires

TABLE II. Seismoelectric reflection and transmission coefficients for $\theta=30°$ at $f=10$ Hz and $f=500$ kHz.

	$f=10$ Hz	$f=500$ kHz
$T_E^{Pf,Pf}$	4.6700×10^{-1}	4.7334×10^{-1}
$T_E^{Ps,Ps}$	1.8083×10^{-3}	1.3026×10^{-1}
$T_E^{TM,TM}$	-2.6500×10^{-10}	-4.9895×10^{-7}
$T_E^{SV,SV}$	1.3084×10^{-1}	7.0295×10^{-2}
$T_E^{Pf,Ps}$	-2.0028×10^{-10}	-8.0868×10^{-7}
$T_E^{Pf,TM}$	-2.7470×10^{-12}	-2.5059×10^{-9}
$T_E^{Pf,SV}$	7.4887×10^{-11}	3.0585×10^{-7}
$T_E^{Ps,TM}$	6.7059×10^{-10}	5.2570×10^{-7}
$T_E^{Ps,SV}$	-1.0420×10^{-8}	-3.7939×10^{-5}
$T_E^{TM,SV}$	4.3970×10^{-14}	1.0814×10^{-7}
$R_E^{E,E}$	7.4497×10^{-11}	1.1871×10^{-7}
$R_E^{Pr,Pr}$	-4.0035×10^{-1}	-3.2615×10^{-1}
$T_E-R_E^{E,E}-R_E^{Pr,Pr}$	1.0000×10^{0}	1.0000×10^{0}

$$\langle Y_3(\mathbf{x},t)\rangle - \langle Y_3^{fl}(\mathbf{x},t)\rangle^{E,E} - \langle Y_3^{fl}(\mathbf{x},t)\rangle^{Pr,Pr} = \langle Y_3^{fl}(\mathbf{x},t)\rangle^{Pin,Pin}. \quad (50)$$

Introducing energy transmission coefficients, e.g., $T_E=\langle Y_3(\mathbf{x},t)\rangle/\langle Y_3^{fl}(\mathbf{x},t)\rangle^{Pin,Pin}$, we write

$$T_E - R_E^{E,E} - R_E^{Pr,Pr} = 1. \quad (51)$$

We note, again, that T_E consists of four orthodox flux transmission coefficients and six interference flux transmission coefficients. Numerical examples are given in Tables II and III. In Table II, the angle of incidence θ is fixed at 30° and frequencies f of 10 Hz (left column) and 500 kHz (right column) are chosen. Higher frequencies favor seismoelectric conversion. In Table III, the angular frequency is fixed at 10^6 rad/s, and angles of incidence $\theta=30°$ (left column) and $\theta=45°$ (right column) are chosen. Equation (51) is satisfied indeed. $T_E^{Pf,Ps}$ and $T_E^{Ps,SV}$ are negative, because of the out-of-phase behavior of the slow P-wave. $R_E^{Pr,Pr}$ is negative, because the reflected acoustic pressure and fluid displacement have opposite phase. $T_E^{Pf,Pf}$ approaches zero for $\theta=45°$ because this angle is beyond the critical angle of incidence of the fast P-wave.

TABLE III. Seismoelectric reflection and transmission coefficients for $\omega=10^6$ rad/s at $\theta=30°$ and $\theta=45°$.

	$\theta=30°$	$\theta=45°$
$T_E^{Pf,Pf}$	4.7389×10^{-1}	1.6454×10^{-7}
$T_E^{Ps,Ps}$	1.2478×10^{-1}	2.7971×10^{-1}
$T_E^{TM,TM}$	-5.0880×10^{-7}	-1.6581×10^{-6}
$T_E^{SV,SV}$	7.2674×10^{-2}	6.6128×10^{-1}
$T_E^{Pf,Ps}$	-2.6036×10^{-6}	3.2114×10^{-5}
$T_E^{Pf,TM}$	-3.3667×10^{-9}	4.4496×10^{-9}
$T_E^{Pf,SV}$	9.8734×10^{-7}	5.2354×10^{-5}
$T_E^{Ps,TM}$	7.1950×10^{-7}	2.4385×10^{-6}
$T_E^{Ps,SV}$	-1.2373×10^{-4}	1.9413×10^{-3}
$T_E^{TM,SV}$	1.3113×10^{-7}	8.4593×10^{-7}
$R_E^{E,E}$	1.3503×10^{-7}	5.4312×10^{-7}
$R_E^{Pr,Pr}$	-3.2877×10^{-1}	-5.6982×10^{-2}
$T_E-R_E^{E,E}-R_E^{Pr,Pr}$	1.0000×10^{0}	1.0000×10^{0}

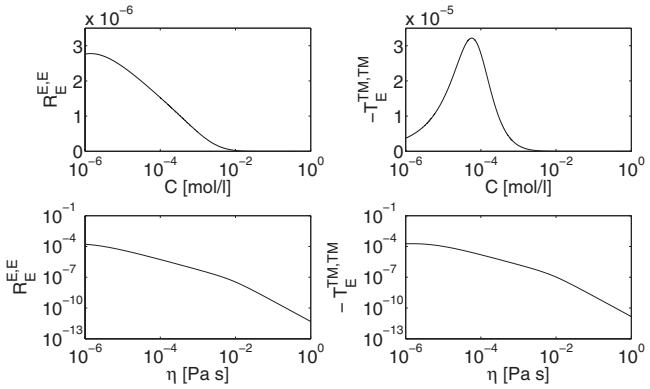

FIG. 4. Variation of $R_E^{E,E}$ and $T_E^{TM,TM}$ as a function of electrolyte concentration (C) and pore fluid viscosity (η) at $\omega=10^6$ rad/s and $\theta=45°$.

B. Parameter variations

Seismoelectric conversions are generated at contrasts in (i) elastic properties (e.g., elastic moduli), (ii) fluid chemistry (pH and electrolyte concentration), and (iii) transport properties such as permeability (Haartsen and Pride, 1997). Electrolyte concentration (C), pore fluid viscosity (η), and permeability (k_0) are dominant seismoelectric conversion parameters while pH, pore fluid bulk modulus (K_f), porosity (ϕ), and tortuosity (α_∞) influence the seismoelectric conversion to a smaller extent (see also Haartsen and Pride, 1997; Mikhailov *et al.*, 2000; Garambois and Dietrich, 2002; Bordes *et al.*, 2006). We investigate the variation of $R_E^{E,E}$ and $T_E^{TM,TM}$ as a function of these parameters in Figs. 4–7 at fixed angular frequency and angle of incidence: $\omega=10^6$ rad/s and $\theta=45°$.

In Fig. 4, $R_E^{E,E}$ decreases with increasing electrolyte concentration because the absolute value of the zeta-potential decreases, which reduces the electrokinetic coupling, as can be seen from Eq. (A4). $T_E^{TM,TM}$ peaks around $C=10^{-4}$ mol/l. This behavior is related to the vertical electrokinetic energy flux, which depends on the TM-wave velocity. We found that the corresponding maximum attenuation of this wave is at $C=10^{-4}$ mol/l.

Both coefficients strongly decrease with increasing fluid viscosity. This is intuitively explained because a low viscosity will favor EM-wave generation as fluid circulation is enhanced, as was noted by Garambois and Dietrich (2002).

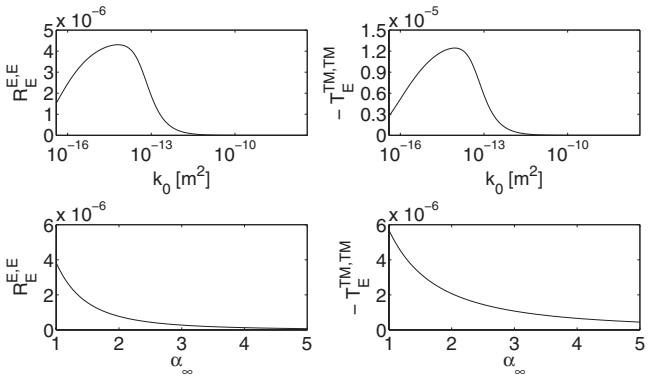

FIG. 5. Variation of $R_E^{E,E}$ and $T_E^{TM,TM}$ as a function of permeability (k_0) and tortuosity (α_∞) at $\omega=10^6$ rad/s and $\theta=45°$.

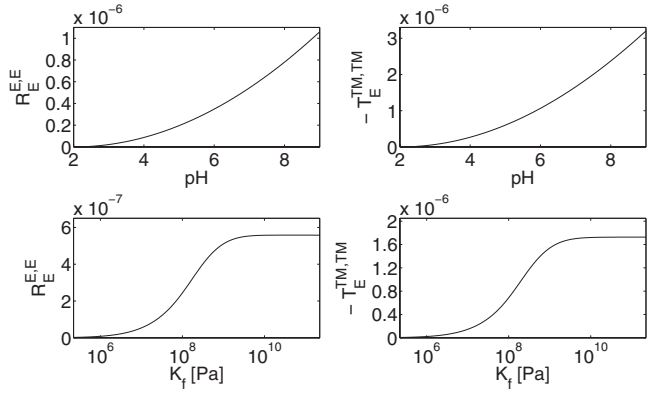

FIG. 6. Variation of $R_E^{E,E}$ and $T_E^{TM,TM}$ as a function of pH and bulk modulus of the pore fluid (K_f) at $\omega=10^6$ rad/s and $\theta=45°$.

In the upper two graphs of Fig. 5 we see that seismoelectric coefficients vary over several orders of magnitude as a function of the permeability k_0. This behavior is attributed to the influence of k_0 on the electrokinetic coupling coefficient $L(\omega)$. From Eq. (A3) we see that by increasing permeability we also increase the pore volume-to-surface ratio Λ, which has two competing effects on $L(\omega)$. Initially the length scale of Λ approaches the characteristic length of the electric double layer d so that $L(\omega)$ increases with increasing Λ. For permeabilities larger than 10^{-14} m^2 the influence of Λ^2 in the denominator of $L(\omega)$ becomes dominant so that the seismoelectric coefficients decrease. The effect of tortuosity on the seismoelectric coefficients is shown in the lower two graphs of Fig. 5. Tortuosity also influences $L(\omega)$, but its effect is smaller than that of k_0 because of its smaller variability. Again, increasing tortuosity effectively increases Λ. For these parameter value combinations, d/Λ is always negligible so that the seismoelectric coefficients decrease with increasing tortuosity.

$R_E^{E,E}$ and $T_E^{TM,TM}$ increase approximately linearly with pH (upper two graphs of Fig. 6), which is a result of the linear relation used for the zeta-potential [see Eq. (A5)]. Also $L(\omega)$ is directly proportional to ζ [see Eq. (A4)].

In the lower two graphs of Fig. 6, we notice that as the pore fluid becomes stiffer, seismoelectric coefficients $R_E^{E,E}$ and $T_E^{TM,TM}$ increase toward a limiting value for large pore fluid bulk moduli. This increase corresponds with a larger contrast in seismoelectric properties across the interface as the compressional wave velocities increase with increasing incompressibility of the pore fluid.

$R_E^{E,E}$ and $T_E^{TM,TM}$ as a function of porosity ϕ are shown in Fig. 7. The increase with porosity of both seismoelectric coefficients is explained by the fact that $L(\omega)$ depends approximately linearly on ϕ [see Eq. (A4)], implying that an increase in surface area increases electrokinetic coupling.

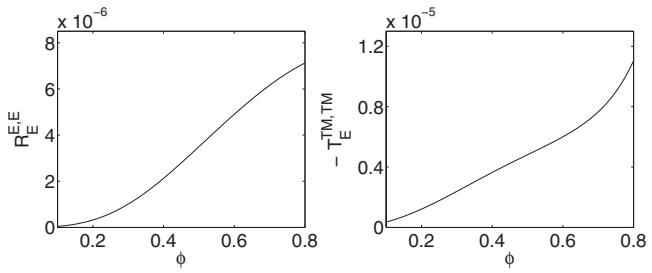

FIG. 7. Variation of $R_E^{E,E}$ and $T_E^{TM,TM}$ as a function of porosity (ϕ) at $\omega=10^6$ rad/s and $\theta=45°$.

This sensitivity analysis indicates that for a water-saturated natural sandstone, electrolyte concentration, pore fluid viscosity, and permeability should be sufficiently low ($C\leq 10^{-3}$ mol/l, $\eta\leq 10^{-3}$ Pa s, and $k_0\leq 10^{-12}$ m^2), and the pH sufficiently high (say pH=7 or more) in order to have appreciable seismoelectric conversion.

V. CONCLUSIONS

The dispersion relations for seismoelectric wave propagation in poroelastic media were solved in terms of effective densities. This allows an elegant incorporation of both viscous and electrokinetic coupling in the effective densities. We solved the seismoelectric reflection and transmission coefficients at a fluid/porous-medium boundary. The dependence of the reflected and transmitted EM-waves due to an incident fluid wave on angle of incidence and frequency was shown. Recasting seismoelectric reflection and transmission coefficients to vertical energy fluxes, while accounting for orthodox and interference fluxes, it was asserted that energy conservation is obeyed. For a water/shallow-sandstone interface, seismoelectric conversion at 10 Hz is on the order 10^{-10} and at 500 kHz it is on the order 10^{-7} for energy flux coefficients. A sensitivity analysis was performed. Electrolyte concentration, pore fluid viscosity, and permeability were varied within realistic ranges and it was shown that this influenced seismoelectric conversions over several orders of magnitude. This sensitivity analysis allows the possibility to devise experiments in which the seismoelectric effect can be detected. Moreover, it allows us to appreciate the use of the electrokinetic effect as an exploration technique that is complementary to conventional seismic surveys for exploring hydrocarbon reserves.

ACKNOWLEDGMENTS

The authors thank Christiaan Schoemaker for fruitful discussions and Evert Slob for in-depth comments. This work was performed under the financial support of Shell-FOM within the research program "The physics of fluids and sound propagation."

APPENDIX A: DYNAMIC COEFFICIENTS

The dynamic permeability $k(\omega)$ is given by (Johnson *et al.*, 1987)

$$k(\omega)=k_0\left[\sqrt{1+i\frac{\omega}{\omega_t}\frac{M}{2}}+i\frac{\omega}{\omega_t}\right]^{-1}, \tag{A1}$$

where k_0 is permeability. The transition frequency ω_t and the similarity parameter M are given by

$$\omega_t=\frac{\phi\eta}{\alpha_\infty k_0\rho_f}, \tag{A2}$$

$$M = \frac{8\alpha_\infty k_0}{\phi\Lambda^2}, \tag{A3}$$

where α_∞ is the tortuosity and Λ is a weighted pore volume-to-surface ratio. The electrokinetic coupling coefficient $L(\omega)$ is obtained from Pride's (1994) theory

$$L(\omega) = -\frac{\phi}{\alpha_\infty}\frac{\varepsilon_0\epsilon_f\zeta}{\eta}\left(1-2\frac{d}{\Lambda}\right) \times\left[1+2i\frac{\omega}{M\omega_t}\left(1-2\frac{d}{\Lambda}\right)^2\left(1+d\sqrt{\frac{i\omega\rho_f}{\eta}}\right)^2\right]^{-1/2}, \tag{A4}$$

where d is the Debye length (defined below) and ζ is the zeta-potential. A semi-empirical relationship between the zeta-potential, electrolyte concentration (C), and pH is used (Pride and Garambois, 2005) as follows:

$$\zeta = [0.010 + 0.025\ \log_{10}(C)]\frac{\mathrm{pH}-2}{5}. \tag{A5}$$

The dynamic conductivity $\sigma(\omega)$ is given by

$$\sigma(\omega) = \frac{\phi\sigma_f}{\alpha_\infty}\left[1+\frac{2[C_{\mathrm{em}}+C_{\mathrm{os}}(\omega)]}{\sigma_f\Lambda}\right], \tag{A6}$$

where σ_f is conductivity of the pore fluid, C_{em} is excess conductance associated with electromigration of excess charge, and $C_{\mathrm{os}}(\omega)$ is excess conductance associated with electroosmosis. Expressions for σ_f, C_{em}, and $C_{\mathrm{os}}(\omega)$ are

$$\sigma_f = \sum_{l=1}^{N_i}(ez_l)^2 b_l N_l, \tag{A7}$$

$$C_{\mathrm{em}} = 2d\sum_{l=1}^{N_i}(ez_l)^2 b_l N_l\left[\exp\left(-\frac{ez_l\zeta}{2k_BT}\right)-1\right], \tag{A8}$$

$$C_{\mathrm{os}}(\omega) = \frac{(\varepsilon_0\epsilon_f)^2\zeta^2}{2d\eta}P\left[1+\frac{2}{P}d\sqrt{\frac{i\omega\rho_f}{\eta}}\right]^{-1}, \tag{A9}$$

$$P = \frac{8k_BTd^2}{\varepsilon_0\epsilon_f\zeta^2}\sum_{l=1}^{N_i}N_l\left[\exp\left(-\frac{ez_l\zeta}{2k_BT}\right)-1\right], \tag{A10}$$

$$d = \sqrt{\left[\sum_{l=1}^{N_i}\frac{(ez_l)^2N_l}{\varepsilon_0\epsilon_f k_BT}\right]^{-1}}, \tag{A11}$$

where k_B is Boltzmann's constant, e is electron charge, T is temperature, and N_l is the amount of species l ions per volume. In this article we consider a binary symmetric electrolyte (N_i=2; z_1=−z_2=1; N_1=N_2) with mobilities b_1 and b_2 (see Table I).

APPENDIX B: ELEMENTS OF $\underline{\underline{\mathbf{A}}}$

Applying the boundary conditions for the seismoelectric reflection and transmission problem yields a linear system

$$\underline{\underline{\mathbf{A}}}\cdot(R^E,R^M,T^{Pf},T^{Ps},T^{TM},T^{SV})^T = (k_3^{fl},\phi\rho_{fl},0,0,0,0)^T, \tag{B1}$$

where elements of matrix $\underline{\underline{\mathbf{A}}}$ are

$$\begin{aligned}
A(1,1) &= 0,\\
A(1,2) &= k_3^{fl},\\
A(1,3) &= k_3^{Pf}[1-\phi+\phi\beta^{Pf}(\omega)],\\
A(1,4) &= k_3^{Ps}[1-\phi+\phi\beta^{Ps}(\omega)],\\
A(1,5) &= k_1[1-\phi+\phi\beta^{TM}(\omega)],\\
A(1,6) &= k_1[1-\phi+\phi\beta^{SV}(\omega)],
\end{aligned} \tag{B2}$$

$$\begin{aligned}
A(2,1) &= 0,\\
A(2,2) &= -\phi\rho_{fl},\\
A(2,3) &= [Q+R\beta^{Pf}(\omega)]s_{Pf}^2(\omega),\\
A(2,4) &= [Q+R\beta^{Ps}(\omega)]s_{Ps}^2(\omega),\\
A(2,5) &= 0,\\
A(2,6) &= 0,
\end{aligned} \tag{B3}$$

$$\begin{aligned}
A(3,1) &= 0,\\
A(3,2) &= 0,\\
A(3,3) &= k_1k_3^{Pf},\\
A(3,4) &= k_1k_3^{Ps},\\
A(3,5) &= k_1^2-\frac{\omega^2}{2}s_{TM}^2(\omega),\\
A(3,6) &= k_1^2-\frac{\omega^2}{2}s_{SV}^2(\omega),
\end{aligned} \tag{B4}$$

$$\begin{aligned}
A(4,1) &= 0,\\
A(4,2) &= 0,\\
A(4,3) &= k_1^2-\omega^2s_{Pf}^2(\omega)\frac{N_1(\omega)}{2G},\\
A(4,4) &= k_1^2-\omega^2s_{Ps}^2(\omega)\frac{N_2(\omega)}{2G},\\
A(4,5) &= -k_1k_3^{TM},\\
A(4,6) &= -k_1k_3^{SV},
\end{aligned} \tag{B5}$$

$$A(5,1) = -\frac{1}{\mu_{fl}} s_E^2(\omega),$$

$$A(5,2) = 0,$$

$$A(5,3) = 0,$$

$$A(5,4) = 0,$$

$$A(5,5) = \frac{\alpha^{TM}(\omega)}{\mu} s_{TM}^2(\omega),$$

$$A(5,6) = \frac{\alpha^{SV}(\omega)}{\mu} s_{SV}^2(\omega), \tag{B6}$$

$$A(6,1) = -k_3^E,$$

$$A(6,2) = 0,$$

$$A(6,3) = k_1 \alpha^{Pf}(\omega),$$

$$A(6,4) = k_1 \alpha^{Ps}(\omega),$$

$$A(6,5) = -k_3^{TM} \alpha^{TM}(\omega),$$

$$A(6,6) = -k_3^{SV} \alpha^{SV}(\omega), \tag{B7}$$

where $N_1(\omega) = P - Q(1-\phi)/\phi + [Q - R(1-\phi)/\phi]\beta^{Pf}(\omega)$, $N_2(\omega) = P - Q(1-\phi)/\phi + [Q - R(1-\phi)/\phi]\beta^{Ps}(\omega)$, and $s_E(\omega)$ is the slowness of the electromagnetic wave in the fluid, which can be calculated using $s_E^2(\omega) = (\omega^2 \mu_{fl} \varepsilon_0 \epsilon_{fl} - i\omega\mu_{fl}\sigma_{fl})/\omega^2$ (Nabighian and Corbett, 1988) with upper fluid layer permeability, relative permittivity, and conductivity denoted by μ_{fl}, ϵ_{fl}, and σ_{fl}, respectively.

Allard, J. F. (**1993**). *Propagation of Sound in Porous Media* (Elsevier Applied Science, London).

Biot, M. A. (**1956a**). "Theory of propagation of elastic waves in a fluid-saturated porous solid. I. Low-frequency range," J. Acoust. Soc. Am. **28**, 168–178.

Biot, M. A. (**1956b**). "Theory of propagation of elastic waves in a fluid-saturated porous solid. II. Higher frequency range," J. Acoust. Soc. Am. **28**, 179–191.

Biot, M. A., and Willis, D. G. (**1957**). "The elastic coefficients of the theory of consolidation," ASME J. Appl. Mech. **24**, 594–601.

Block, G. I., and Harris, J. G. (**2006**). "Conductivity dependence of seismoelectric wave phenomena in fluid-saturated sediments," J. Geophys. Res. **111**, B01304.

Bordes, C., Jouniaux, L., Dietrich, M., Pozzi, J.-P., and Garambois, S. (**2006**). "First laboratory measurements of seismo-magnetic conversions in fluid-filled Fontainebleau sand," Geophys. Res. Lett. **33**, L01302.

Butler, K. E., Russell, R. D., Kepic, A. W., and Maxwell, M. (**1996**). "Measurement of the seismoelectric response from a shallow boundary," Geophysics **61**, 1769–1778.

Denneman, A. I. M., Drijkoningen, G. G., Smeulders, D. M. J., and Wapenaar, K. (**2002**). "Reflection and transmission of waves at a fluid/porous-medium interface," Geophysics **67**, 282–291.

Deresiewicz, H., and Skalak, R. (**1963**). "On uniqueness in dynamic poroelasticity," Bull. Seismol. Soc. Am. **53**, 783–788.

Dutta, N. C., and Odé, H. (**1983**). "Seismic reflections from a gas-water contact," Geophysics **48**, 148–162.

(**1988**). *Electromagnetic Methods in Applied Geophysics—Theory*, edited by M. N. Nabighian and J. D. Corbett (Society of Exploration Geophysicists, Tulsa, OK), Vol. **1**.

Garambois, S., and Dietrich, M. (**2001**). "Seismoelectric wave conversions in porous media: Field measurements and transfer function analysis," Geophysics **66**, 1417–1430.

Garambois, S., and Dietrich, M. (**2002**). "Full waveform numerical simulations of seismoelectromagnetic wave conversions in fluid-saturated stratified porous media," J. Geophys. Res. **107**, ESE5.1–ESE5.18.

Haartsen, M. W. (**1995**). "Coupled electromagnetic and acoustic wavefield modeling in poro-elastic media and its applications in geophysical exploration," Ph.D. thesis, Massachusetts Institute of Technology, Cambridge, MA.

Haartsen, M. W., and Pride, S. R. (**1997**). "Electroseismic waves from point sources in layered media," J. Geophys. Res. **102**, 24745–24769.

Haines, S. S., and Pride, S. R. (**2006**). "Seismoelectric numerical modeling on a grid," Geophysics **71**, N57–N65.

Haines, S. S., Pride, S. R., Klemperer, S. L., and Biondi, B. (**2007**). "Seismoelectric imaging of shallow targets," Geophysics **72**, G9–G20.

Han, Q., and Wang, Z. (**2001**). "Time-domain simulation of SH-wave-induced electromagnetic field in heterogeneous porous media: A fast finite-element algorithm," Geophysics **66**, 448–461.

Johnson, D. L., Koplik, J., and Dashen, R. (**1987**). "Theory of dynamic permeability and tortuosity in fluid-saturated porous media," J. Fluid Mech. **176**, 379–402.

Mikhailov, O. V., Haartsen, M. W., and Toksöz, M. N. (**1997**). "Electroseismic investigation of the shallow subsurface: Field measurements and numerical modeling," Geophysics **62**, 97–105.

Mikhailov, O. V., Queen, J., and Toksöz, M. N. (**2000**). "Using borehole electroseismic measurements to detect and characterize fractured (permeable) zones," Geophysics **65**, 1098–1112.

Pride, S. R. (**1994**). "Governing equations for the coupled electromagnetics and acoustics of porous media," Phys. Rev. B **50**, 15678–15696.

Pride, S. R., and Garambois, S. (**2005**). "Electroseismic wave theory of Frenkel and more recent developments," J. Eng. Mech. **131**, 898–907.

Pride, S. R., and Haartsen, M. W. (**1996**). "Electroseismic wave properties," J. Acoust. Soc. Am. **100**, 1301–1315.

Santos, J. E., Corbero, J. M., Ravazzoli, C. L., and Hensley, J. L. (**1992**). "Reflection and transmission coefficients in fluid-saturated porous media," J. Acoust. Soc. Am. **91**, 1911–1923.

Thompson, A. H., and Gist, G. A. (**1993**). "Geophysical applications of electrokinetic conversion," The Leading Edge **12**, 1169–1173.

Thompson, A. H., Hornbostel, S., Burns, J., Murray, T., Raschke, R., Wride, J., McCammon, P., Sumner, J., Haake, G., Bixby, M., Ross, W., White, B. S., Zhou, M., and Peczak, P. (**2007**). "Field tests of electroseismic hydrocarbon detection," Geophysics **72**, N1–N9.

White, B. S., and Zhou, M. (**2006**). "Electroseismic prospecting in layered media," SIAM J. Appl. Math. **67**, 69–98.

Zhu, Z., Toksöz, M. N., and Burns, D. R. (**2008**). "Electroseismic and seismoelectric measurements of rock samples in a water tank," Geophysics **73**, E153–E164.